NO Disproportionation Reactivity of Fe Tropocoronand Complexes

Katherine J. Franz and Stephen J. Lippard*

Contribution from the Department of Chemistry, Massachusetts Institute of Technology, Cambridge, Massachusetts 02139

Received May 19, 1999

Abstract: The synthesis and characterization of divalent [Fe(TC-5,5)] **(1)** and trivalent [Fe(OTf)(TC-5,5)] **(2)** tropocoronand complexes are described. Compound **1** reacts with 1 equiv of NO to form the $\{FeNO\}^7$ complex **3**. A single-crystal X-ray structure determination of **3** reveals a trigonal bipyramidal geometry with a linearly coordinated nitrosyl (Fe−N−O = 174.3(4)°) having a short Fe−N distance of 1.670(4) Å. EPR and Mössbauer spectroscopy, SQUID susceptometry, and normal coordinate analysis indicate **3** to be a low-spin $\{Fe^{III}(NO^-)\}^{2+}$ species. In the presence of excess NO, **3** converts to a metastable nitrosyl−nitrito complex that decomposes by losing NO_2, which subsequently nitrates the aromatic tropolone rings of the ligand. The final products of the NO disproportionation reaction are N_2O and [Fe(NO)(TC-5,5-NO_2)] **(4)**. The ν_{NO} stretching band of **4** is increased to 1716 cm^{-1} from its value of 1692 cm^{-1} in **3**, owing to the electron-withdrawing nitro groups on the ligand, and the compound no longer promotes the disproportionation of NO. Mechanistic aspects of the reaction are discussed.

Introduction

The conversion of NO into species such as NO_2, N_2O_3, $OONO^-$, and N_2O, has important biological[1] and environmental[2] consequences. Some of these transformations occur by direct oxidation, but transition metal ions are often required to activate nitric oxide. The disproportionation of NO is effected by a variety of metal complexes,[3,4] including those of iron,[5] ruthenium,[6,7] cobalt[8,9] and copper.[10−12]

We recently reported novel NO disproportionation chemistry promoted by a manganese tropocoronand (Figure 1) complex [Mn(THF)(TC-5,5)].[13] When the stoichiometry of NO addition was carefully controlled, the nitrosyl complex [Mn(NO)(TC-5,5)] could be isolated. This complex further reacts with NO to yield N_2O and the nitrito derivative [Mn(NO_2)(TC-5,5)]. The strongly donating nature of the tropocoronand ligand, coupled with its geometric constraints that convey trigonal bipyramidal geometry at the metal center,[14] provide the framework for this novel manganese nitrosyl reactivity, in which the coordinated NO ligand is reductively activated.

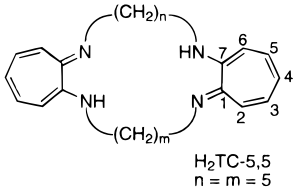

Figure 1. H_2TC-5,5 ligand.

To explore the generality of this chemistry, we studied the reaction of NO with the corresponding [Fe(TC-5,5)] complex. As described here, a discrete iron nitrosyl complex forms which, like its Mn analogue, also promotes NO disproportionation but with some interesting and unexpected differences. The iron complexes also provide the additional opportunity to apply Mössbauer spectroscopy for characterizing formal oxidation levels. Mechanistic details of the disproportionation reaction are discussed that delineate the reaction pathways of these two different metal complexes. The results provide a useful benchmark for evaluating the possible roles of Mn and Fe complexes in processing NO in naturally occurring systems.

Experimental Section

General Information. All reactions were carried out under nitrogen in a glovebox or by using standard Schlenk techniques. Pentane, tetrahydrofuran (THF), and 2-methyltetrahydrofuran (Me-THF) were freshly distilled from sodium benzophenone ketyl under nitrogen. Dichloromethane and dichloroethane were distilled from CaH_2 under nitrogen. The ligand H_2(TC-5,5)[15] and [Fe($OTf)_2$($CH_3CN)_2$][16] were synthesized as described in the literature. Nitric oxide (Matheson, 99%) and ^{15}NO (Aldrich, 99%) were purified of higher nitrogen oxides by passage through a column of NaOH pellets and a mercury bubbler and kept over mercury in gas storage bulbs. Analysis by GC of the NO used in the experiments revealed no contaminants, such as NO_2 or N_2O, at the limit of the thermal conductivity detector, about 30 nM. All other reagents were obtained commercially and not further purified. UV−

(1) Marnett, L. J. *Chem. Res. Toxicol.* **1996**, *9*, 807−808.
(2) Trogler, W. C. *J. Chem. Educ.* **1995**, *72*, 973−976.
(3) Bottomley, F. *Reactions of Coordinated Ligands*; Plenum: New York, 1989; Vol. 2, pp 115−222.
(4) Richter-Addo, G. B.; Legzdins, P. *Metal Nitrosyls*; Oxford University: New York, 1992.
(5) Yoshimura, T. *Inorg. Chim. Acta* **1984**, *83*, 17−21.
(6) Lorković, I. M.; Ford, P. C. *Inorg. Chem.* **1999**, *38*, 1467−1473.
(7) Miranda, K. M.; Bu, X.; Lorković, I.; Ford, P. C. *Inorg. Chem.* **1997**, *36*, 4383−4848.
(8) Gans, P. *J. Chem. Soc. A* **1967**, 943−946.
(9) Gwost, D.; Caulton, K. G. *Inorg. Chem.* **1974**, *13*, 414−417.
(10) Ruggiero, C. E.; Carrier, S. M.; Tolman, W. B. *Angew. Chem., Int. Ed. Engl.* **1994**, *33*, 895−897.
(11) Paul, P. P.; Karlin, K. D. *J. Am. Chem. Soc.* **1991**, *113*, 6331−6332.
(12) Schneider, J. L.; Carrier, S. M.; Ruggiero, C. E.; Young, V. G., Jr.; Tolman, W. B. *J. Am. Chem. Soc.* **1998**, *120*, 11408−11418.
(13) Franz, K. J.; Lippard, S. J. *J. Am. Chem. Soc.* **1998**, *120*, 9034−9040.
(14) Jaynes, B. S.; Ren, T.; Masschelein, A.; Lippard, S. J. *J. Am. Chem. Soc.* **1993**, *115*, 5589−5599.
(15) Davis, W. M.; Roberts, M. M.; Zask, A.; Nakanishi, K.; Nozoe, T.; Lippard, S. J. *J. Am. Chem. Soc.* **1985**, *107*, 3864−3870.
(16) Bryan, P. S.; Dabrowiak, J. C. *Inorg. Chem.* **1975**, *14*, 296−299.

10.1021/ja991664f CCC: $18.00
Published on Web 10/21/1999

visible spectra were recorded on a Cary 1 E spectrophotometer. Mass spectra were determined in 3-nitrobenzyl alcohol matrix on a Finnegan 4000 mass spectrometer with 70-ev impact ionization.

Synthetic Procedures. [Fe(TC-5,5)] (1). A portion of H_2TC-5,5 (502 mg, 1.33 mmol) was doubly deprotonated in 10 mL of THF with *n*-BuLi (1.75 mL, 2.80 mmol of 1.6 M solution in hexanes) to give an orange solution. The solution immediately turned burgundy red upon addition of $[Fe(OTf)_2(CH_3CN)_2]$ (638 mg, 1.46 mmol). After the solution stirred for 2.5 h, THF was removed in vacuo, and the resulting powder was twice triturated with pentane and then extracted into CH_2Cl_2 and filtered through Celite. The solvent was again removed in vacuo, and the product was triturated twice with 3 mL of pentane. Dark burgundy prisms of X-ray quality crystals were grown by pentane diffusion into a THF solution of the complex. Yield: 340 mg, 60%. FTIR (KBr): 1586 (s), 1503 (s), 1466, 1451, 1407 (s), 1387, 1363, 1330, 1265 (s), 1228 (s), 1193, 1130, 1048 (s), 990, 936, 885, 721 (s), 484 cm^{-1}. UV−vis (THF) nm (M^{-1} cm^{-1}): 277 (48000), 388 (37000), 425 (21000). $\mu_{eff} = 5.19\ \mu_B$ (300 K). Mössbauer $\delta = 0.66(1)$ mm/s, $\Delta E_Q = 1.18(1)$ mm/s. Anal. Calcd for $FeC_{24}H_{30}N_4$: C, 66.98; H, 7.03; N, 13.02. Found: C, 66.74; H, 7.11; N, 12.79.

[Fe(OTf)(TC-5,5)] (2). An equivalent of AgOTf (93 mg, 0.361 mmol) was added to a 5-mL THF solution of **1** (154 mg, 0.358 mmol); the color changed from red-orange to darker red. Solid Ag metal was removed by filtration after 0.5 h, and the solvent was evaporated. X-ray quality crystals were grown from pentane diffusion into a THF solution of the complex. Yield: 161 mg, 78%. FTIR (KBr): 1584, 1501 (s), 1433, 1410, 1384, 1339, 1314, 1264, 1225, 1200, 1166, 1044, 1023 (s), 885, 731, 632 (s) cm^{-1}. UV−vis (THF) nm (M^{-1} cm^{-1}) 274 (50000), 354 (19400), 388 (19700), 467 (13400), 500 (14200), 805 (7500). $\mu_{eff} = 5.95\ \mu_B$ (300 K). EPR: $g' = 8.69, 5.27, 4.25$. Mössbauer δ_{major} (>92%) = 0.27(1) mm/s, $\Delta E_Q = 2.19(1)$ mm/s. $\delta_{minor} = -0.01(3)$ mm/s, $\Delta E_Q = 0.56(3)$ mm/s. Anal. Calcd for $FeC_{25}H_{30}N_4O_3F_3S$: C, 51.82; H, 5.22; N, 9.67. Found: C, 51.60; H, 5.13; N, 9.37.

[Fe(NO)(TC-5,5)] (3). A portion of **1** (110 mg, 0.256 mmol) was dissolved in 10 mL of THF in a 25-mL, thick-walled, round-bottom flask equipped with a screw-top Teflon stopcock and a sidearm for attachment to a high-vacuum manifold. This red solution was subjected to three freeze−pump−thaw cycles before NO gas (0.307 mmol) was transferred under reduced pressure to the solution. Submerging the reaction flask in a liquid N_2 bath facilitated the complete transfer of NO. The color remained deep red upon exposure to NO. The reaction was allowed to stir for 2 h as the solution warmed to room temperature. The solvent was removed in vacuo, and X-ray quality crystals were grown in the drybox by pentane diffusion into a THF solution of the complex. Yield: 81 mg, 67%. FTIR (KBr): 1692 (s, ν_{NO}), 1582 (s), 1503 (s), 1412, 1342, 1264, 1231, 1089, 1044, 1018, 978, 936, 886, 870, 799, 727, 582, 555, 532, 522, 515, 475, 432 cm^{-1}. FTIR (THF) 1710 (s, ν_{NO}). UV−vis (THF) nm (M^{-1} cm^{-1}): 277 (25100), 420 (14700), 515 (5200). $\mu_{eff} = 2.40\ \mu_B$ (300 K). EPR: $g = 2.11, 2.03, 2.01$. Mössbauer $\delta = 0.06(1)$ mm/s, $\Delta E_Q = 1.39(1)$ mm/s. Anal. Calcd for $FeC_{24}H_{30}N_5O$: C, 62.61; H, 6.57; N, 15.21. Found: C, 62.17; H, 6.88; N, 14.66.

[Fe(NO)(TC-5,5-NO$_2$)] (4). A portion of **1** (65 mg, 0.151 mmol) was dissolved in 10.0 mL of THF in a 25-mL septum-sealed Schlenk flask. The solution was cooled to −78 °C over a dry ice/acetone slush bath, and purified NO was purged through the solution for 5 min. After 1 h at −78 °C, the cold bath was allowed to warm slowly to room temperature; the reaction was left sealed and stirring for 12 h. The solvent was removed in vacuo, and the black residue was extracted into dichloroethane in the glovebox to give a deep purple solution after some insoluble black material was filtered away. Blackish-purple needles suitable for X-ray analysis were grown from pentane diffusion into a dichloroethane solution. Yield: 25 mg, 30%. FTIR (KBr): 1716 (s, ν_{NO}), 1588, 1504, 1278, 1242, 1063, 1043, 873, 822, 737, 530, 474 cm^{-1}. FTIR (THF) 1727 (s, ν_{NO}). UV−vis (THF) nm (M^{-1} cm^{-1}): 267 (26000), 432 (20000), 522 (25000). Mössbauer $\delta = -0.02(1)$ mm/s, $\Delta E_Q = 1.26(1)$ mm/s. EPR: $g = 2.14, 2.03, 2.01$. Anal. Calcd for $FeC_{24}H_{29}N_6O_3$: C, 57.04; H, 5.76; N, 16.63. Calcd for $FeC_{24}H_{28}N_7O_5$: C, 52.27; H, 5.31; N, 17.78. Found: C, 52.21, 52.82, 51.46; H, 5.18, 4.99, 5.11; N, 15.67, 15.78, 15.95.

Magnetic Susceptibility. Variable temperature magnetic susceptibilities were measured with a Quantum Design MPMS SQUID susceptometer. The samples were loaded in a drybox in gel capsules and suspended in plastic straws. Field dependence studies at 5 and 150 K showed a linear correlation of magnetization vs field strength from 0 to 10 000 G for all compounds. The data were collected at 5000 G in the temperature range from 5 to 300 K. The infrared spectrum of **2** following the measurement was unchanged, confirming that the sample had not oxidized during the procedures required to obtain the data. The susceptibilities of the straw and gel capsule were measured at the same field and temperatures for accurate correction of their contribution to the total measured susceptibility. The diamagnetic contributions from the ligands were calculated from Pascal's constants[17] and applied. The effective magnetic moments (μ_{eff}) were calculated from the expression, $\mu_{eff} = 2.828(\chi T)^{1/2}$.

Electrochemistry. Cyclic voltammetry was performed in a nitrogen-filled glovebox with an EG&G model 263 potentiostat. A standard three-electrode setup was used, consisting of a $Ag/AgNO_3$ reference electrode (0.01 M in acetonitrile), a platinum wire auxiliary electrode, and a 1.75 mm^2 platinum disk working electrode. The solute samples were generally 2 mM in freshly distilled CH_2Cl_2 and 0.2 M in supporting electrolyte $(Bu_4N)(PF_6)$, triply recrystallized from acetone. All spectra were externally referenced to ferrocene under identical conditions, for which $E_{1/2} = 180$ mV vs $Ag/AgNO_3$ in CH_2Cl_2.

^{57}Fe Mössbauer Spectroscopy. Samples for ^{57}Fe Mössbauer spectroscopy were finely ground, intimately mixed in Apiezon-N grease, and then kept in a cryostat at 77 K during measurement. A ^{57}Co/Rh source was moved at constant acceleration at room temperature against the absorber samples. All isomer shift (δ) and quadrupole splitting (ΔE_Q) values are reported with respect to ^{57}Fe-enriched metallic iron foil that was used for velocity calibration. The displayed spectra were folded to enhance the signal-to-noise ratio. Best fits for the data were calculated by using the MBF Mössbauer plot and fit program.[18]

EPR Spectroscopy. EPR spectra were recorded as frozen Me−THF glasses on a Bruker model 300 ESP X-band spectrometer operating at 9.47 GHz and running WinEPR software. Low temperatures were maintained with a liquid He Oxford Instruments EPR 900 cryostat. The following temperatures and powers were used for particular compounds: **2**, 26 K, 10 mW; **3**, 4 K, 0.1 mW; **4**, 10 K, 1.0 mW.

IR Spectroscopy. Standard IR spectra were recorded on a Bio Rad FTS-135 instrument with Win-IR software. Solid samples were pressed into KBr pellets; solution samples were prepared in an airtight Graseby-Specac solution cell with CaF_2 or KBr windows. In situ IR sample monitoring was performed with a ReactIR 1000 from ASI Applied Systems equipped with a 1-in. diameter, 30-reflection silicon ATR (SiComp) probe optimized for maximum sensitivity. In a typical reaction, the IR probe was inserted through a nylon adapter and O-ring seal into an oven-dried, custom-made cylindrical flask equipped with a gas-inlet adapter, a septum-sealed joint and a stir bar. The reaction vessel was deaerated by three vacuum-fill cycles with Ar. Under Ar, the flask was charged with 5 mL of the appropriate solvent, usually THF, and background spectra were recorded at room temperature and/or at −78 °C by placing the flask over a dry ice/acetone slush bath. The solvent was removed in vacuo, and a 5-mL solution of sample (10−20 mM) was injected under Ar and cooled to −78 °C. The NO purification train, which extended from the gas tank regulator through a mercury bubbler and solid NaOH column into the reaction flask through a needle inserted into a rubber septum, was pre-purged with Ar. The reaction was monitored through ReactIR 2.0 software. After a few initial background spectra were recorded, the Ar flow was terminated and replaced by a constant flow of NO into the headspace of the reaction at a sufficient rate to ensure an immediate excess of NO atmosphere.

Vibrational Analysis. Normal-mode analysis was performed on a Silicon Graphics Indigo workstation with the Svib program.[19] Cartesian coordinates for the Fe−N−O fragment were obtained from the X-ray

(17) Carlin, R. L. *Magnetochemistry*; Springer-Verlag: New York, 1986.
(18) Nagel, S. MBF Mössbauer Plot and Fit Program. 890330/c; Philipps Universität; Marburg, Germany.
(19) Mukherjee, A.; Spiro, T. G. Program 656, Bulletin Quantum Chemistry Program Exchange. Indiana University; 1995.

Table 1. Summary of X-ray Crystallographic Data

compound	[Fe(TC-5,5)] **1**	[Fe(OTf)(TC-5,5)] **2**	[Fe(NO)(TC-5,5)] **3**
formula	$FeC_{24}H_{30}N_4$	$FeC_{25}H_{30}N_4O_3F_3S$	$FeC_{24}H_{30}N_5O$
formula wt (g mol^{-1})	430.37	579.44	460.38
crystal system	hexagonal	monoclinic	monoclinic
space group	$P6_522$	$P2_1/n$	$P2_1/c$
a (Å)	11.0367(4)	15.4688(2)	9.210(3)
b (Å)		9.4959(2)	10.096(5)
c (Å)	30.423(1)	18.5944(2)	23.334(8)
α (deg)			
β (deg)		113.551(1)	94.58(3)
γ (deg)			
V (Å^3)	3209.3(2)	2503.83(7)	2163.0 (1)
Z	6	4	4
ρ_{calcd} (g cm^{-1})	1.336	1.537	1.414
absorption coeff (mm^{-1})	0.722	0.744	0.724
temp (K)	188(2)	188(2)	188(2)
radiation λ (Å)	0.71073	0.71073	0.71073
reflections collected	20224	14175	12772
data/parameter	2602/133	5715/454	4919/280
R[a]	0.0796	0.0623	0.0608
wR2[b]	0.1491	0.1434	0.1768
crystal size (mm)	0.66 × 0.24 × 0.14	0.40 × 0.25 × 0.15	0.34 × 0.14 × 0.03
max/min peak (e/Å^3)	0.267/−0.453	0.889/−0.505	0.859/−0.422

[a] $R = \Sigma||F_o| - |F_c||/\Sigma|F_o|$. [b] $wR^2 = \{\Sigma[w(F_o^2 - F_c^2)^2]/\Sigma[w(F_o^2)^2]\}^{1/2}$.

structures of **3** and **4** and input to the program to generate potential energy matrixes. Incorporating force constants, the program constructs and solves the vibrational secular equation.[20] The three principal and three interaction force constants associated with the MNO oscillator were refined by least-squares fitting of the experimental frequencies. For **3**, these values were 1692, 582, 515 cm^{-1} for ^{14}NO and 1660, 579, and 509 cm^{-1} for ^{15}NO. For **4** these values were 1716, 737, 530 for ^{14}NO and 1686, 721, 522 for ^{15}NO.

GC Headspace Analysis. Procedures for the detection and quantitation of N_2O have been described previously.[13]

X-ray Crystallography. Single crystals were mounted on quartz fibers with Paratone N (Exxon) and transferred rapidly to the −85 °C cold stream of a Bruker (formerly Siemens) CCD X-ray diffraction system controlled by a Pentium-based PC running the SMART software package.[21] The general procedures for data collection and reduction followed those reported elsewhere.[22] Empirical absorption corrections were calculated and applied from the SADABS program.[23] Structures were solved by the direct methods program XS, and refinements were carried out with XL, both part of the SHELXTL program package.[24] Non-hydrogen atoms were refined by a series of least-squares cycles. All hydrogen atoms in **1** and **3** were assigned idealized positions and given a thermal parameter 1.2 times that of the carbon atom to which each was attached. The hydrogen atoms of compound **2** were located in difference Fourier maps and refined isotropically. The structure of **1** was refined in the chiral space group $P6_522$ and assigned the correct absolute configuration. The Flack[25] absolute structure parameter was 0.09(6), compared to expected values of 0.0 for the correct and +1.0 for the inverted structure. Crystallographic information is provided in Table 1, and Figures S1−S3 (Supporting Information) display the structures with complete atom labeling schemes.

Results and Discussion

Synthesis and Characterization. An investigation of iron tropocoronand complexes and their reaction with nitric oxide was undertaken, and the results were compared with those previously described for the manganese analogue.[13] The iron(II) complex **1** was synthesized in good yield by reaction of $[Fe(OTf)_2(CH_3CN)_2]$ with the dilithium salt of TC-5,5 in THF. The distorted tetrahedral stereochemistry of this complex, which has crystallographically required C_2 symmetry, is depicted as an ORTEP plot in Figure 2. Selected bond distance and angle information is contained in Table 2. Previously we demonstrated that profound changes in the stereochemistry of transition metal tropocoronand complexes attend alterations in the number of polymethylene linker chains of length n and m in the TC-n,m ligand (Figure 1).[15,26−28] To relieve the strain imposed on the pentamethylene chains of the TC-5,5 ligand upon metal chelation, the two five-membered chelate ring planes must twist away from planarity. For Co^{II}, Ni^{II}, and Cu^{II} TC-5,5 complexes, the dihedral angle Θ, which measures the degree of twist, is 69.9,[28] 70.1,[15] and 61.3°,[27] respectively. Compound **1** has a Θ value of 66.0°, within that range. This ligand-imposed distorted tetrahedral geometry in **1** differs from the square-planar geometry encountered in most Fe(II) complexes of other tetraazamacrocyclic ligands. Porphyrins,[29,30] phthalocyanins,[31]

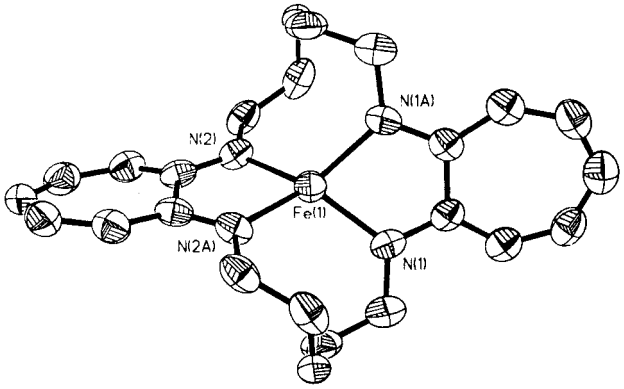

Figure 2. ORTEP diagram of [Fe(TC-5,5)] **1** showing selected atom labels and 50% probability ellipsoids for all non-hydrogen atoms.

(20) Wilson, E. B.; Decius, J. C.; Cross, P. C. *Molecular Vibrations*; McGraw-Hill: New York, 1955.
(21) SMART. 4.0; Bruker Analytical X-ray Systems; Madison, WI, 1996.
(22) Feig, A. L.; Bautista, M. T.; Lippard, S. J. *Inorg. Chem.* **1996**, *35*, 6892−6898.
(23) Program written by Professor George Sheldrick at the University of Göttingen which corrects data collected on Bruker CCD and multiwire detectors for absorption and decay.
(24) SHELXTL: Structure Analysis Program. 5.1; Bruker Analytical X-ray Systems; Madison, WI, 1997.
(25) Flack, H. D. *Acta Crystallogr.* **1983**, *A44*, 499−506.
(26) Doerrer, L. H.; Lippard, S. J. *Inorg. Chem.* **1997**, *36*, 2554−2563.
(27) Davis, W. M.; Zask, A.; Nakanishi, K.; Lippard, S. J. *Inorg. Chem.* **1985**, *24*, 3737−3743.
(28) Jaynes, B. S.; Doerrer, L. H.; Liu, S.; Lippard, S. J. *Inorg. Chem.* **1995**, *34*, 5735−5744.
(29) Collman, J. P.; Hoard, J. L.; Kim, N.; Lang, G.; Reed, C. A. *J. Am. Chem. Soc.* **1975**, *97*, 2676−2681.

Table 2. Selected Bond Distances and Angles[a]

cmpd	distances	(Å)	angles	(deg)
1	Fe−$N_{(TC)avg}$	2.020(3)	N1−Fe−N1A	80.2(3)
			N1A-Fe−N2	114.8(2)
			N2−Fe−N2A	79.6(3)
			N1−Fe−N2	139.0(2)
2	Fe−$N_{(TC)avg}$	2.009(6)	N3−Fe−N1	168.0(2)
	Fe−O1	2.117(3)	N2−Fe−O1	120.3(2)
			N4−Fe−O1	129.0(2)
			N4−Fe−N2	110.0(2)
			N3−Fe−O1	89.9(1)
			N1−Fe−O1	85.1(1)
3	Fe−$N_{(TC)avg}$	1.96(2)	N3−Fe−N1	172.0(2)
	Fe−NO	1.670(4)	N2−Fe−N5	129.9(2)
	N5−O1	1.176(5)	N5−Fe−N4	130.7(2)
			N4−Fe−N2	99.4(2)
			Fe−N5−O1	174.3(4)
			N3−Fe−N5	92.3(2)
			N1−Fe−N5	95.6(2)

[a] Numbers in parentheses are estimated standard deviations of the last significant figure. Atoms are labeled as indicated in Figures 2, 5, and 7.

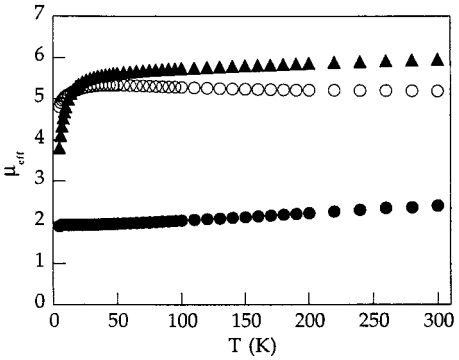

Figure 3. Effective magnetic moments from 5 to 300 K for ○ [Fe(TC-5,5)] **1**, ▲ [Fe(OTf)(TC-5,5)] **2**, and ● [Fe(NO)(TC-5,5)] **3**.

and others[32,33] afford square-planar complexes that exhibit unusual intermediate-spin ($S = 1$) ground states and short Fe−N bond distances, <2.00 Å.[29] In contrast, the average Fe−N bond distance in **1** is 2.020(3) Å, and the effective magnetic moment μ_{eff}, as shown in Figure 3, is 5.19 μ_B at 300 K, consistent with an $S = 2$ ground state. The Mössbauer spectrum, displayed in Figure 4a, reveals an isomer shift δ of 0.66(1) mm/s, a value in the range of high-spin ferrous complexes.[34]

Compound **1** can be oxidized with AgOTf in THF to afford [Fe(OTf)(TC-5,5)] (**2**) in high yield. In a manner similar to that observed for 4-coordinate [M(TC-*n*,*m*)] complexes, which twist from square-planar to tetrahedral geometry as *n* and *m* increase, 5-coordinate [M(X)(TC-*n*,*m*)] complexes vary from square pyramidal to trigonal bipyramidal geometry.[35] The ORTEP diagram in Figure 5 and metrical data in Table 2 reveal that **2** assumes the expected trigonal bipyramidal geometry of 5-coordinate TC-5,5 complexes, with the triflate anion being coordinated in the equatorial plane. Figure 3 displays the temperature

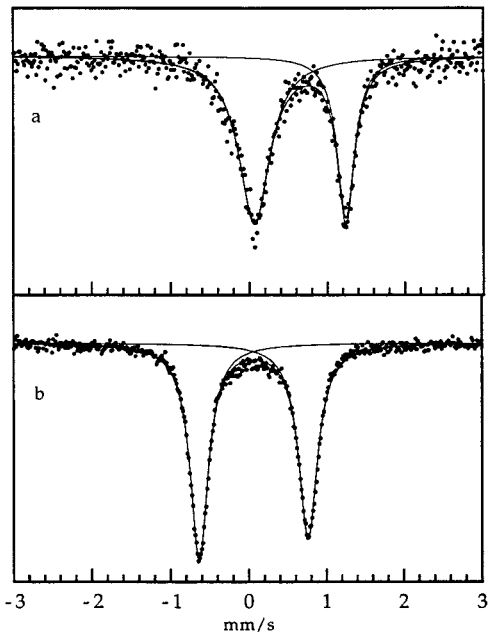

Figure 4. Mössbauer spectra of (a) [Fe(TC-5,5)] **1**, $\delta = 0.66(1)$ mm/s, $\Delta E_Q = 1.18(1)$ mm/s and (b) [Fe(NO)(TC-5,5)] **3**, $\delta = 0.06(1)$ mm/s, $\Delta E_Q = 1.39(1)$ mm/s. Both spectra were recorded as solid samples at 77 K.

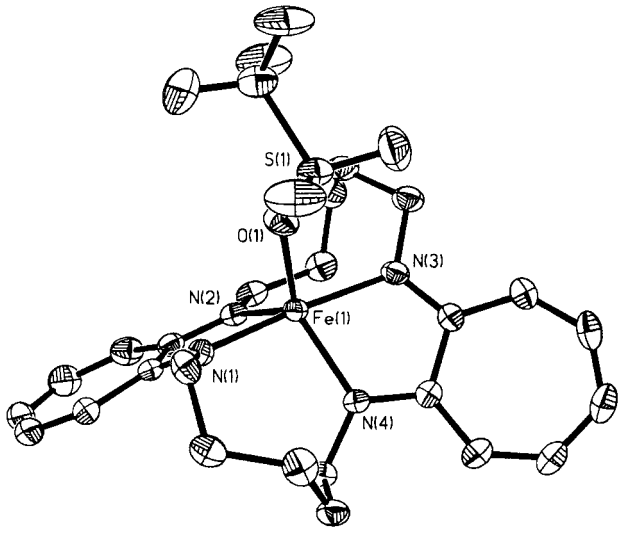

Figure 5. ORTEP diagram of [Fe(OTf)(TC-5,5)] **2** showing selected atom labels and 50% probability ellipsoids for all non-hydrogen atoms.

dependence of the effective magnetic moment, μ_{eff}, which ranges from 5.49 to 5.95 μ_B for $30 < T < 300$ K. The latter value is in excellent agreement with that expected for an $S = 5/2$ spin-only ion. The rapid decrease in μ_{eff} below 30 K is consistent with zero-field splitting effects.[17] The EPR spectrum of **2** (Figure 6) displays a sharp signal at effective $g' = 8.69$ together with a multicomponent resonance centered at $g' = 4.3$. The spectrum is consistent with high-spin Fe(III) in a noncubic coordination environment, in which the magnetic levels in the absence of an external magnetic field comprise three Kramers doublet states, each of which may be described by a set of three effective g' values.[36] The signal at $g' \approx 9$ arises from the lowest doublet in one principal direction, and the multicomponent signal at $g' \approx 4.3$ arises from the middle doublet in more than one principal direction.[37] The highest doublet is often not observed.[37]

(30) Strauss, S. H.; Silver, M. E.; Long, K. M.; Thompson, R. G.; Hudgens, R. A.; Spartalian, K.; Ibers, J. A. *J. Am. Chem. Soc.* **1985**, *107*, 4207−4215.

(31) Kirner, J. F.; Dow, W.; Scheidt, W. R. *Inorg. Chem.* **1976**, *15*, 1685−1690.

(32) Goedken, V. L.; Pluth, J. J.; Peng, S.-M.; Bursten, B. *J. Am. Chem. Soc.* **1976**, *98*, 8014−8021.

(33) Little, R.; Ibers, J. A.; Baldwin, J. E. *J. Am. Chem. Soc. 97*, 7049−7053.

(34) Dickson, D. P. E.; Berry, F. J. *Mossbauer Spectroscopy*; Cambridge University: New York, 1986.

(35) Jaynes, B. S.; Ren, T.; Liu, S.; Lippard, S. J. *J. Am. Chem. Soc.* **1992**, *114*, 9670−9671.

(36) Pilbrow, J. R. *Transition Ion Electron Paramagnetic Resonance*; Oxford University: New York, 1990.

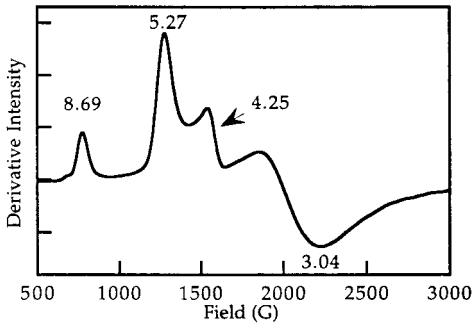

Figure 6. EPR spectrum of [Fe(OTf)(TC-5,5)] **2** in Me-THF glass at 26 K, 10 mW and 9.4 GHz.

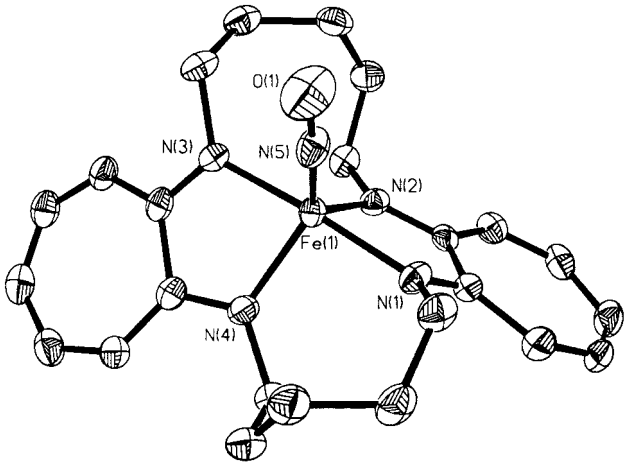

Figure 7. ORTEP diagram of [Fe(NO)(TC-5,5)] **(3)** showing selected atom labels and 50% probability ellipsoids for all non-hydrogen atoms.

Table 3. Comparison of Selected $S = {}^1/_2$ {FeNO}^{7} Complexes

	ν_{NO}, cm^{-1}	M−N(NO), Å	N−O, Å	M−N−O, deg	S	ref
[Mn(NO)(TC-5,5)]	1662	1.6993(3)	1.179(3)	174.1(3)	2	13
[Fe(NO)(TC-5,5)]	1692	1.670(4)	1.176(5)	174.3(4)	$^1/_2$	*a*
[Fe(NO)(TPP)]^b	1670	1.717(7)	1.12 (1)	149.2(6)	$^1/_2$	58
[Fe(NO)(salen)]^c	1630	1.80(15)	1.15	132.(5)	$^1/_2$	48
[Fe(NO)L]^d	1636	1.716(11)	1.17(2)	144.1(9)	$^1/_2$	50
[FeNO(TMC)]$^{2+}$ ^{e}	1840	1.737(6)	1.137(6)	177.5(5)	*e*	39

^{a} This work. ^{b} TPP = tetraphenylporphyrin. ^{c} Data from −175 °C, at rt this compound is $S = {}^3/_2$. ^{d} L = tetramethyldibenzotetraazacyclotetradecine. ^{e} TMC = tetramethylcyclam; this complex has a $S = {}^1/_2$ to $^3/_2$ spin-equilibrium.

When **1** reacts with one equivalent of NO in solution, the mononitrosyl compound **3** forms, the structure of which is shown in Figure 7 (see also Table 2). Solutions of this nitrosyl complex are stable to vigorous Ar purging, vacuum and refluxing in toluene, but rapidly oxidize in air. The Fe−N−O metrical parameters are listed in Table 3, where they are compared with the values from [Mn(NO)(TC-5,5)] as well as other 5-coordinate {FeNO}^{7} species. Of the tabulated iron compounds with ν_{NO} between 1630 and 1690 cm^{-1}, the tropocoronand complex is unique in having a nearly linear Fe−N−O linkage. This difference is related to the geometry at the metal center. Molecular orbital studies for {MNO}^{7} complexes predict a bent Fe−N−O angle if the NO is coordinated in the apical position of a square pyramid.[38] Trigonal bipyramidal geometry, on the other hand, can accommodate a linearly coordinated nitrosyl if the nitrosyl lies in the equatorial plane.[38] As mentioned previously, the constraints of the TC-5,5 ligand

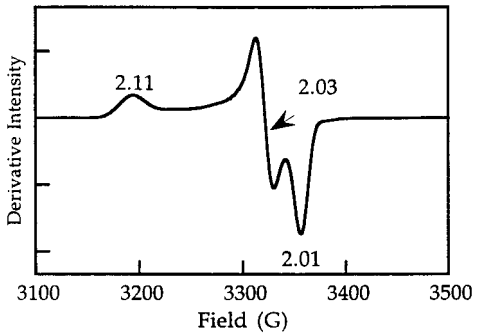

Figure 8. EPR spectrum of [Fe(NO)(TC-5,5)] **3** in Me-THF glass at 4 K, 0.1 mW, 9.4 GHz.

impose trigonal bipyramidal geometry on five-coordinate complexes, where the exogenous ligand lies in the equatorial plane.[13,27,28,35] The linearly coordinated nitrosyl ligand of **3** is in the equatorial plane of a trigonal bipyramid, as evident in Figure 7 and Table 2, thereby reconciling its linear coordination with the low NO stretching frequency. The [Fe(NO)(TMC)]$^{2+}$ complex included in Table 3 also has distorted trigonal bipyramidal geometry and a linearly coordinated nitrosyl.[39] The Fe−N_{NO} bond distance in **3** is slightly shorter than those in the comparable compounds, implying a rather strong Fe−N bond.

In the literature of {FeNO}^{7} compounds, there are examples of both $S = {}^3/_2$[40−43] and $S = {}^1/_2$[44−47] ground states, as well as several compounds that exhibit spin-crossover behavior.[39,48,49] Various physical methods were employed to probe the electronic and magnetic properties of **3**, from which we conclude that it is an $S = {}^1/_2$ species having no spin-crossover behavior. Figure 3 reveals that μ_{eff} remains nearly constant from 5 to 300 K, ranging from 1.89 to 2.40 μ_B. These values are only slightly higher than the 1.73 μ_B spin-only value expected for an $S = {}^1/_2$ compound. The EPR spectrum of **3**, shown in Figure 8, displays g values at 2.11, 2.03, and 2.01, closely resembling those of other $S = {}^1/_2$ {FeNO}^{7} compounds.[44,46] An $S = {}^1/_2$ value can arise either from a low-spin Fe(II) with the unpaired electron on the nitrosyl ligand, as occurs in [Fe(NO)(TPP)],[45] or from a formally low-spin Fe(III) ($S = {}^1/_2$) coupled antiferromagnetically

(37) Peisach, J.; Blumberg, W. E.; Lode, E. T.; Coon, M. J. *J. Biol. Chem.* **1971**, *246*, 5877−5881.

(38) Hoffmann, R.; Chen, M. M. L.; Elian, M.; Rossi, A. R.; Mingos, D. M. P. *Inorg. Chem.* **1974**, *13*, 2666−2675. The {MNO}^{n} notation denotes the number of electrons (n) in the MNO unit as the sum of the d electrons of the metal plus the electrons in π^* orbitals of NO [Enemark, J. H.; Feltham, R. D. *Coord. Chem. Rev.* **1974**, *13*, 339−406.

(39) Hodges, K. D.; Wollmann, R. G.; Kessel, S. L.; Hendrickson, D. N.; Van Derveer, D. G.; Barefield, E. K. *J. Am. Chem. Soc.* **1979**, *101*, 906−917.

(40) Brown, C. A.; Pavlosky, M. A.; Westre, T. E.; Zhang, Y.; Hedman, B.; Hodgson, K. O.; Solomon, E. I. *J. Am. Chem. Soc.* **1995**, *117*, 715−732.

(41) Zhang, Y.; Pavlosky, M. A.; Brown, C. A.; Westre, T. E.; Hedman, B.; Hodgson, K. O.; Solomon, E. I. *J. Am. Chem. Soc.* **1992**, *114*, 9189−9191.

(42) Shepherd, R. E.; Sweetland, M. A.; Junker, D. E. *J. Inorg. Biochem.* **1997**, 1−14.

(43) Ray, M.; Golombek, A. P.; Hendrich, M. P.; Yap, G. P. A.; Liable-Sands, L. M.; Rheingold, A. L.; Borovik, A. S. *Inorg. Chem.* **1999**, *38*, 3110−3115.

(44) Nasri, H.; Ellison, M. K.; Chen, S.; Huynh, B. H.; Scheidt, W. R. *J. Am. Chem. Soc.* **1997**, *119*, 6274−6283.

(45) Wayland, B. B.; Olson, L. W. *J. Am. Chem. Soc.* **1974**, *96*, 6037−6041.

(46) Chen, Y.; Sweetland, M. A.; Shepherd, R. E. *Inorg. Chim. Acta* **1997**, *260*, 163−172.

(47) Hauser, C.; Wieghardt, K. Thesis, Ruhr-University Bochum, 1998.

(48) Haller, K. J.; Johnson, P. L.; Feltham, R. D.; Enemark, J. H. *Inorg. Chim. Acta* **1979**, *33*, 119−130.

(49) Wells, F. V.; McCann, S. W.; Wickman, H. H.; Kessel, S. L.; Hendrickson, D. N.; Feltham, R. D. *Inorg. Chem.* **1982**, *21*, 2306−2311.

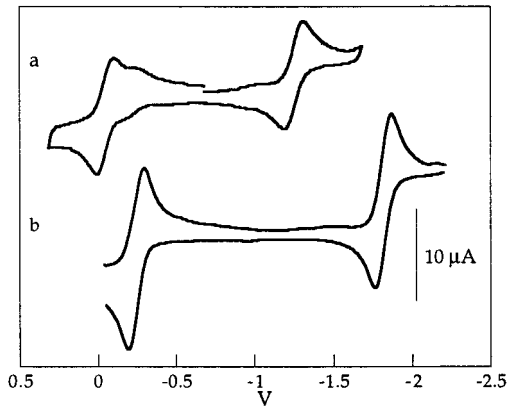

Figure 9. Cyclic voltammograms of (a) [Fe(NO)(TC-5,5-NO_2)] **4**, with $E_{1/2} = -1.24$ V and -0.046 V and (b) [Fe(NO)(TC-5,5)] **3**, with $E_{1/2} = -1.81$ V and -0.24 V, referenced to Cp_2Fe/Cp_2Fe^+.

with NO^- ($S = 1$), as was favored for another tetraazamacrocyclic FeNO complex.[50]

To probe further the nature of the iron center in **3**, a Mössbauer spectrum was measured at 77 K. The results are shown in Figure 4b. As a general trend, a low isomer shift reflects increased formal charge on iron. Moreover, low-spin compounds tend to have smaller δ values than their high-spin counterparts.[34] The low δ of 0.06(1) mm/s of **3** places it well below the 0.66(1) mm/s of the high-spin Fe(II) compound **1**, as well as the 0.27(1) mm/s value of the high-spin Fe(III) compound **2** (Figure S4). The Mössbauer data suggest that iron has been oxidized to Fe(III) in compound **3**. The shorter average $Fe-N_{TC}$ bond distance of 1.96(2) Å in **3** compared to the values of 2.020(3) Å in **1**, an Fe(II) species, and 2.009(6) Å in high-spin ferric **2**, is also consistent with oxidation of iron to afford low-spin Fe(III).

Assignment of the iron center as Fe(III) implies that the coordinated nitrosyl has been formally reduced to NO^-. To evaluate further such an assignment, a normal coordinate analysis was performed to extract the force constants of the Fe−N−O fragment. The nitrosyl stretching vibration for [Fe(NO)(TC-5,5)] appears at 1692 cm^{-1} and shifts to 1660 cm^{-1} upon isotopic labeling with ^{15}NO, in agreement with the 1662 cm^{-1} value computed by assuming a classical diatomic oscillator model. By using six experimental frequencies (1692, 582, 515 cm^{-1} for ^{14}NO and 1660, 579, and 509 cm^{-1} for ^{15}NO), the force constants were adjusted by least-squares refinement until the calculated and experimental values matched one another. The results indicate that, apart from the assignment of the high-frequency mode to the N−O stretch, the band at 579 cm^{-1} derives from the Fe−N−O bend and that at 509 cm^{-1} from the Fe−N stretch. The force constant derived for the N−O stretch, 11.41(4) mdyne/Å, reflects NO^- character, the force constants of NO^-, NO, and NO^+ being 8.4, 15.5, and 21.3 mdyne/Å, respectively.[40] Combined with the physical data presented above, the results support the formal assignment of **3** as low-spin $\{Fe^{III}(NO^-)\}^{2+}$.

Electrochemical investigation of compound **3** revealed two reversible redox couples, as indicated by the cyclic voltammogram in Figure 9b. A reversible reduction occurs at -1.81 V, and a reversible oxidation appears at -0.24 V vs Cp_2Fe/Cp_2Fe^+. Attempts to reduce **3** chemically to afford an $\{FeNO\}^8$ species did not lead to any isolable product. Oxidation of **3** with $[Cp_2Fe]OTf$ in THF, on the other hand, did afford a product consistent with the formulation [Fe(NO)(TC-5,5)(OTf)]. Reaction of 1 equiv of NO with the triflate complex **2** provides an alternative route to this $\{FeNO\}^6$ species, which has an NO stretch at 1707 cm^{-1} ($\nu^{15}_{NO} = 1675$ cm^{-1}) in the solid state, 15 cm^{-1} higher in energy than that of the parent nitrosyl complex **3**.

(50) Berno, P.; Floriani, C.; Chiesi-Villa, A.; Guastini, C. *J. Chem. Soc., Dalton Trans.* **1988**, 1409−1412.

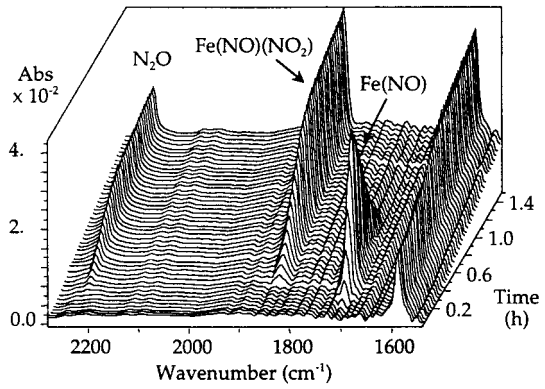

Figure 10. In situ IR reaction spectra of [Fe(TC-5,5)] **1** in THF at −78 °C as NO is introduced into the headspace of the reaction flask. The label "FeNO" signifies the ν_{NO} of [Fe(NO)(TC-5,5)] **3** at 1710 cm^{-1}, whereas "Fe(NO)(NO_2)" represents the ν_{NO} of the nitrosyl−nitrito species at 1850 cm^{-1}. N_2O appears at 2223 cm^{-1}.

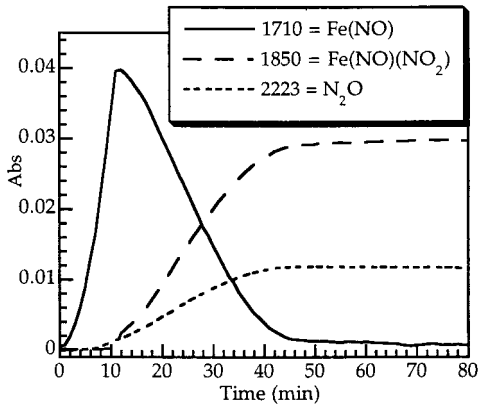

Figure 11. Profile traces of absorbance vs time of the relevant IR bands from Figure 10.

Reactivity. We previously reported that [Mn(THF)(TC-5,5)] converts to [Mn(NO)(TC-5,5)] in the presence of NO before reacting further to disproportionate NO, releasing N_2O and forming [Mn(NO_2)(TC-5,5)].[13] The iron nitrosyl compound **3** is structurally and electronically very similar to its Mn analogue. They have both been characterized as $\{M^{III}(NO^-)\}^{2+}$ species with nearly the same N−O bond stretching force constants. It was therefore of interest to determine whether **1** would also promote the disproportionation of NO. Figure 10 displays the results of in situ IR monitoring of the reaction of **1** in THF at −78 °C under an NO atmosphere. The characteristic ν_{NO} of compound **3** appears at 1710 cm^{-1}, and after it reaches its maximum intensity, two new bands emerge, one at 1850 cm^{-1} and one at 2223 cm^{-1}. The latter band corresponds to the formation of N_2O. It takes about 30 min for **3** to be completely consumed, during which time the two new bands reach their maximum intensities and level off. This behavior is revealed by the speciation profiles in Figure 11. The band at 1850 cm^{-1} corresponds to *cis*-[Fe(NO)(NO_2)(TC-5,5)]. The infrared spectrum was inconclusive in distinguishing the NO_2 ligand coordination mode as either N-bound nitro or O-bound nitrito. Although *cis*-nitrosyl−nitro iron complexes are known,[51,52] we favor the nitrosyl−nitrito formulation by analogy with the

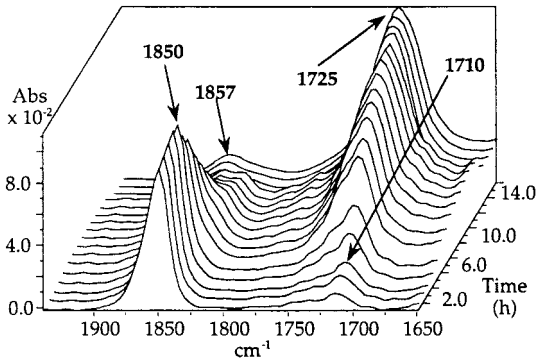

Figure 12. Continuation of the reaction shown in Figure 10 when the solution warms from −78 °C to room temperature. The band at 1710 cm^{-1} corresponds to ν_{NO} of [Fe(NO)(TC-5,5)] **3**, which reappears as the reaction warms, but shifts to 1725 cm^{-1} as **3** is nitrated to form **4**. The band at 1850 cm^{-1} corresponds to the nitrosyl−nitrito species. The residual peak at 1857 cm^{-1} is assumed to be some nitrosyl−nitrito species in which the ligand rings have been nitrated.

corresponding [Mn(NO)(NO_2)(TC-5,5)] complex, for which a crystal structure revealed the O-linked nitrito ligand.[13]

Up to the formation of this intermediate species, the reaction pathways of the Mn and Fe systems appear to be identical. A major difference occurs, however, when the solution warms to room temperature. As shown in Figure 12, a band at 1710 cm^{-1} reappears upon warming that shifts to 1725 cm^{-1}. Concomitantly, the band at 1850 cm^{-1} diminishes in intensity and shifts to 1857 cm^{-1}. After 14 h, a weak band persists in solution at 1857 cm^{-1}, although it decreases upon purging with Ar or evacuation, whereas the strong nitrosyl stretch at 1725 cm^{-1} persists.

The final product from the reaction of **1** with excess NO was determined to be [Fe(NO)(TC-5,5-NO_2)], **4**, an {FeNO}^{7} species in which one or both rings of the tropocoronand ligand have been nitrated. Whereas the intermediate [Mn(NO)(NO_2)(TC-5,5)] loses NO to form [Mn(NO_2)(TC-5,5)],[13] the analogous [Fe(NO)(NO_2)(TC-5,5)] loses NO_2. The assignment of the nitrating species as gaseous NO_2 was verified by reaction of **3** with NO_2, which afforded **4** as evidenced by IR spectroscopy. X-ray crystallographic studies of **4** provided data that were sufficient to reveal the connectivity of the structure.[53] Disorder of the nitro groups on the 4-position of the ligand rings indicated that some of the compound might be nitrated on both rings. This finding was confirmed by a FAB(+)MS of the organic material that was extracted after acidic hydrolysis of **4**, which confirmed the presence of both singly and doubly nitrated H_2TC-5,5-NO_2. A mixture of products is also evident in the C, H, and N analytical determinations of three distinct preparations.

Since the amount of NO_2 present in the products must match the amount of N_2O generated in the reaction on a molar basis, the headspace gas was sampled by gas chromatography to quantitate the corresponding N_2O. The amounts varied considerably, depending on the reaction conditions, ranging from 0.3 to 1.4 equiv of N_2O per iron. The highest yields were obtained by keeping CH_2Cl_2 solutions of **1** cooled to −78 °C for the first 2 h after introducing NO and then sampling the headspace after 48 h at room temperature in a sealed vessel. Eliminating the cooling stage resulted in decreased N_2O production.

The differing product distributions based on reaction temperature can be explained by the in situ IR experiments shown in Figures 10 and 12. Generation of N_2O coincides with formation of the nitrosyl−nitrito species (ν_{NO} = 1850 cm^{-1}), which is stable at −78 °C, but loses NO_2 at higher temperature. Maximizing the formation of the nitrosyl−nitrito species therefore ensures that 1 equiv each of N_2O and NO_2 are generated. Loss of the NO_2 ligand upon warming regenerates the nitrosyl compound **3**, which can then further react with NO to continue the cycle and generate more N_2O and NO_2, as portrayed in Scheme 1. Under these reaction conditions, the catalytic cycle is quenched by the nitration of **3** to form **4**, which does not react further with NO (step e). When the reaction is executed at room temperature, NO_2 is released much more rapidly, forming **4** before each iron center has had a chance to form the nitrosyl−nitrito intermediate, and thereby limiting the generation of N_2O.

Scheme 1

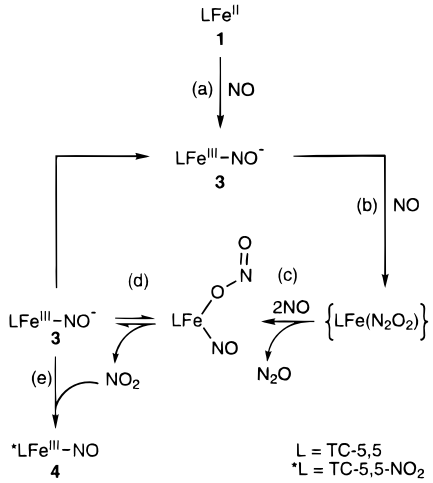

The observation that **4** is incapable of promoting the disproportionation of NO is significant for understanding the factors that affect this reactivity. Compounds **4** and **3** are structurally similar; both are 5-coordinate, mononitrosyl complexes. The electron-withdrawing nitro groups on the TC ligand in **4**, however, decrease the electron density at the iron center, which in turn affects the electronic distribution in the {FeNO}^{7} unit. The cyclic voltammogram of **4**, displayed in Figure 9a, reflects this electronic modulation. Compound **4** is easier to reduce and harder to oxidize than the parent nitrosyl compound **3**. Predictably, the Mössbauer isomer shift (Figure S5) decreases from the value in **3**, consistent with decreased electron density at the metal center.[34] Like its relative **3**, compound **4** is also a low-spin Fe(III) complex, as evidenced by EPR spectroscopy (Figure S5). These subtle changes at the iron center affect the nitrosyl adduct by increasing the energy of the NO stretch. The NO force constant, derived from normal coordinate analysis, is 12.30(2) mdyne/Å, almost a whole unit increase from the value found for **3**. Given the structural similarities of **3** and **4**, we conclude that the decreased electron density at the metal in **4** deactivates the coordinated nitrosyl with respect to electrophilic attack by NO, thereby inhibiting NO disproportionation reactivity. This conclusion corroborates an observation made in a recent study of the NO disproportionation reactivity of various copper tris(pyrazolyl)borate (Tp) complexes. A significant decrease in the rate of NO disproportionation occurred when an electron-withdrawing trifluoromethyl substituted Tp ligand was used.[12]

(51) Ileperuma, O. A.; Feltham, R. D. *Inorg. Chem.* **1977**, *16*, 1876−1883.

(52) Ileperuma, O. A.; Feltham, R. D. *J. Am. Chem. Soc.* **1976**, *98*, 6039−6040.

(53) Crystals were grown by vapor diffusion of pentane into a dichloroethane solution in a glovebox. The structure was determined in space group *Pbcn* with. a = 19.6694(4) Å, b = 12.7979(1) Å, c = 18.5090(3) Å, V = 4659.2(1) Å^3, Z = 8, T = 188(2) K, R = 9.12%, wR^2 = 23.65%.

The reduction of NO to N_2O by iron compounds is not without precedent. $FeSO_4$ is reported to reduce NO_2^- and NO to N_2O in weakly alkaline solutions.[54,55] In bacterial nitrite reductases, heme centers carry out this transformation. Some iron porphyrin complexes also display similar reactivity. Early reports that a dinitrosyl complex forms when [Fe(NO)(TPP)] is exposed to excess NO[45] were later reexamined to disclose a [Fe(NO)(NO_2)(TPP)] species that is stable only in the presence of excess NO.[5] N_2O was also detected in the reaction mixture.[5] Some ruthenium porphyrins also promote NO disproportionation and, in the process, form *trans*-[Ru(P)(NO)(NO_2)] complexes.[6,7]

^{14}NO/^{15}NO Exchange. In an attempt to gain some insight into the mechanism of the disproportionation reaction, in situ IR spectroscopy was used to monitor the reaction of labeled [Fe(^{15}NO)(TC-5,5)] in the presence of excess of ^{14}NO at 1 atm. Figure 13 shows the IR spectra and Figure 14 the time-dependence profiles of the relevant bands. When ^{14}NO is introduced to the reaction, the ν^{15}_{NO} band at 1670 cm^{-1} decreases in intensity and is replaced by the ν^{14}_{NO} band at 1710 cm^{-1}. An increase in bands at 1850 and 2223 cm^{-1} corresponds to the growing concentrations of [Fe(^{14}NO)(NO_2)(TC-5,5)] and $^{14}N^{14}NO$, respectively. A small shoulder can be seen at 1816 cm^{-1}, corresponding to [Fe(^{15}NO)(NO_2)(TC-5,5)]. It is apparent from these results that most of the labeled ^{15}NO is exchanged prior to further reactions. The formation of mixed-label N_2O, as shown in the inset of Figure 13, is therefore the result of this exchange process. The ^{14}NO/^{15}NO exchange reaction, which was also detected in the Mn study,[13] occurs faster than the subsequent reactions that lead to NO disproportionation.

The exchange can be envisioned to occur by either of two different mechanisms, shown in eqs 1−2. The first process is

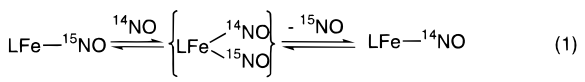

(1)

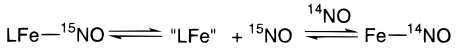

(2)

associative and involves a dinitrosyl intermediate, analogous to that previously proposed for [Mn(NO)(TC-5,5)].[13] Compound **3**, like [Mn(NO)(TC-5,5)], does not lose NO upon purging with N_2 or by heating it in the solid state or in solution in vacuo. The stability of these nitrosyl compounds favors eq 1 over eq 2, although an equilibrium between free and dissociated NO such as in eq 2 cannot be ruled out.

From the mixed-labeling studies it appears that the NO exchange is a pre-equilibrium process that occurs prior to the NO disproportionation reaction. The critical step leading to an N−N bond formation has not been spectroscopically observed. The N−N bond can be envisioned to form in several different ways. A dinitrosyl intermediate could be induced, perhaps by an incoming NO, to collapse and give rise to a hyponitrito M{N(O)NO} species. Alternatively, direct attack of NO on the coordinated nitrosyl would lead to a similar intermediate. Both scenarios have been proposed previously but not definitively proved.[5,8,10,13,56] A dinitrosyl ruthenium porphyrin intermediate was recently reported to form during NO disproportionation.[6] Because of the configurational constraints of the porphyrin ligand, this species would be a *trans*-dinitrosyl and therefore not the direct precursor to N−N bond formation. Although the results of the mixed-labeling studies favor the presence of a *cis*-dinitrosyl intermediate for the NO exchange pathway in [Fe(NO)(TC-5,5)], there is no evidence that such an intermediate leads directly to N−N bond formation. The difference in reactivity between **3** and the electron-deficient **4** and the slowed rates for the electron-deficient [Cu(NO)(Tp)] complex[12] convincingly argue that an electrophilic attack of NO on coordinated NO is a critical aspect in these reactions. The attack could arise either from free NO or from NO that is pre-coordinated to the metal center, such as in a dinitrosyl complex.

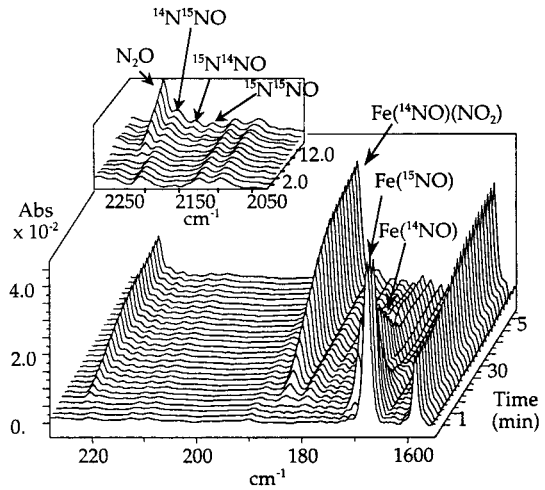

Figure 13. In situ IR reaction spectra of [Fe(^{15}NO)(TC-5,5)] in THF at −78 °C as ^{14}NO is introduced into the headspace of the reaction flask. The label "Fe^{14}NO" signifies the ν^{14}_{NO} of [Fe(^{14}NO)(TC-5,5)] **3** at 1710 cm^{-1}, whereas "Fe^{15}NO" appears at 1670 cm^{-1}. The nitrosyl−nitrito ν^{14}_{NO} appears at 1850 cm^{-1}, and the corresponding ν^{15}_{NO}, which can be seen as a small shoulder alongside the 1850 band, appears at 1816 cm^{-1}. The inset shows the magnified region containing the bands from mixed-labeled N_2O. The assignments were made as follows: $^{14}N^{14}NO$: 2223 cm^{-1}, $^{14}N^{15}NO$: 2200 cm^{-1}, $^{15}N^{14}NO$: 2176 cm^{-1}, and $^{15}N^{15}NO$: 2150 cm^{-1}. The presence of an apparent feature at 2200 cm^{-1} at the beginning of the reaction is an artifact. As the reaction proceeds, the overlapping signal from $^{14}N^{15}NO$ appears well above noise level in this region.

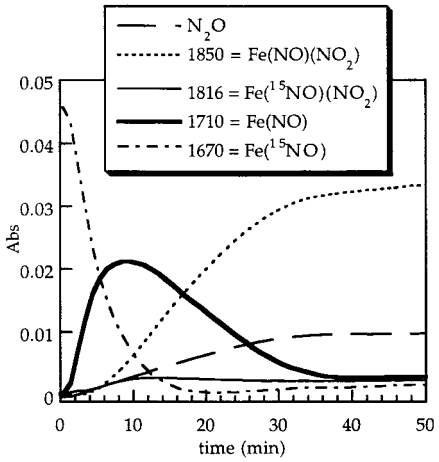

Figure 14. Profile traces of absorbance vs time of the relevant IR bands from Figure 13.

The proposed reaction pathway is outlined in Scheme 1. The first step (a) is the formation of the well-characterized nitrosyl complex **3**. Between steps (a) and (b) is the NO exchange equilibrium, which is not shown explicitly in the scheme, but is most likely by eq 1. Electrophilic attack on the reductively activated nitrosyl ligand of **3** is proposed, yielding an unidentified {Fe(N_2O_2)} intermediate in step (b). Concomitant with the release of N_2O in step (c) is the formation of the nitrosyl−nitrito species that is observable at −78 °C. In step (d) this

(54) Pearsall, K. A.; Bonner, F. T. *Inorg. Chem.* **1982**, *21*, 1978−1985.
(55) Bonner, F. T.; Pearsall, K. A. *Inorg. Chem.* **1982**, *21*, 1973−1978.

species reverts to the original nitrosyl complex **3** by releasing NO_2 upon warming to room temperature. The liberated NO_2 eventually kills the cycle by nitrating the ligand to form the unreactive nitrosyl complex **4** in step (e).

Summary and Conclusions

The iron compound **3** displays interesting reactivity with NO. Geometric constraints of the TC-5,5 ligand lead to trigonal bipyramidal metal nitrosyl complexes in which NO is bound in the equatorial plane; as in the case of Mn,[13] the Fe−N−O linkage is nearly linear. The strongly donating environment of the ligand leads to metal nitrosyl complexes that formally contain oxidized metal centers and reduced coordinated nitrosyl ligands. In the presence of excess NO, both the Mn compound reported previously[13] and the Fe compound reported here promote the disproportionation of NO. During this reaction, metal nitrosyl−nitrito species *cis*-[M(NO)(NO_2)(TC-5,5)] form. The manganese analogue [Mn(NO)(NO_2)(TC-5,5)] loses NO to form [Mn(NO_2)(TC-5,5)], whereas iron retains the NO and loses NO_2, which then reacts to give the final ligand-nitrated [Fe(NO)(TC-55-NO_2)] **4**. The mechanism of the overall reaction involves an NO-exchange step that could go through an equilibrium between bound and dissociated NO, but more likely involves a dinitrosyl intermediate. The steps of the proposed reaction pathway are summarized in Scheme 1. This study strongly supports previous arguments that a coordinated NO^- ligand is required to activate NO reductively to produce N_2O.[57] Modulation of the reduced nature of the coordinated nitrosyl can shut down this process, as is seen for ligand-nitrated **4**. Production of Fe(NO)(NO_2) species and N_2O has been documented in more biologically relevant Fe porphyrins,[5] although the fate of the NO_2 was not investigated. The present study reveals that the decomposition of Fe(NO)(NO_2) species can release the reactive NO_2 radical, a potent agent for cytotoxic DNA- and protein-damaging events.[1] This study also suggests, however, that such reactivity can be controlled by electronic modification of the ligand environment.

Acknowledgment. This work was supported by a grant from the National Science Foundation. We thank Dr. W. Reiff at Northeastern University for the use of his Mössbauer equipment, Mr. D. Lee for his help in running the Mössbauer samples, Dr. B. Spingler for assistance with X-ray crystallography and Dr. R. Davydov for assistance with EPR spectroscopy.

Supporting Information Available: Figures S1−S3 display fully labeled ORTEP diagrams for each reported structure. Figures S4 and S5 contain Mössbauer spectra of **2** and **4**, respectively, and Figure S6 exhibits the EPR spectrum of **4** (PDF). X-ray crystallographic files, in CIF format, are available free of charge via the Internet at http://pubs.acs.org.

JA991664F

(56) MacNeil, J. H.; Berseth, P. A.; Bruner, E. L.; Perkins, T. L.; Wadia, Y.; Westwood, G.; Trogler, W. C. *J. Am. Chem. Soc.* **1997**, *119*, 1668−1675.
(57) McCleverty, J. A. *Chem. Rev.* **1979**, *79*, 53−76.
(58) Scheidt, W. R.; Frisse, M. E. *J. Am. Chem. Soc.* **1975**, *97*, 17−21.